Temperature Droop-Based Dynamic Reactive Power Sharing Technique to Improve the Lifetime of Power Electronic Converter

Anubrata Das, *Student Member, IEEE*, Yugal Gupta, *Student Member, IEEE*, Sandeep Anand, *Senior Member, IEEE*, and Soumya Ranjan Sahoo, *Senior Member, IEEE*

***Abstract*—Thermal stress because of mean junction temperature (T_{jm}) and junction temperature swing (ΔT_j) reduces the lifetime of the power electronic (PE) converters. It is beneficial to distribute the stress evenly among the converters operating in parallel in a system like microgrid to improve their lifetime. The existing techniques usually only distribute stress due to T_{jm}. A few techniques are based on the accumulated damage in PE converters do not necessarily mitigate the effect of ΔT_j. Moreover, most of the the existing techniques are not applicable for nondispatchable energy source like PV. The intermittent nature of active power generation profile of the PV inverter further reduces the lifetime of the PE converters operating in an islanded microgrid. To address this issue, a temperature droop-based dynamic reactive power sharing (TDDRPS) technique is proposed for an islanded ac microgrid to distribute the thermal stress due to both T_{jm} and ΔT_j. The stability of the proposed TDDRPS technique is mathematically analyzed. Finally, the proposed technique is validated through simulation and experimentation on a scaled down laboratory prototype of microgrid.**

***Index Terms*—AC microgrid, junction temperature swing, mean junction temperature, PV, reactive power sharing, temperature droop, thermal stress.**

I. Introduction

POWER electronic (PE) converters (inverter or dc–dc converter) are one of the most fragile components in the system like microgrid. Recent studies [1], [2] show that improving the reliability of the power semiconductor switches, particularly IGBT switches, improves the PE converters' lifetime. The critical stressor behind the failure of switches is thermal stress [3], [4]. Because of this thermal stress, the temperature sensitive parts of the IGBT like the bond wire and the solder joints go through frequent expansion and contraction cycle. As a result, stress and fatigue develop and accumulate in these areas, resulting in failure of IGBT switches. Two factors which quantify the thermal stress are 1) mean junction temperature or steady state temperature (T_{jm}), and 2) junction temperature swing (ΔT_j) [5], [6]. Thermal stress due to ΔT_j occurs very frequently in PE converters operating in a microgrid with nondispatchable energy source like solar photovoltaic (PV). The intermittent nature of active power generation of such sources, results in varying inverter power. Consequently, the power of other parallel connected dispatchable source (battery inverter)-based inverters also varies to maintain the load power demand. This in turn results in the development of stress due to ΔT_j in all the PE converters in the microgrid system. Furthermore, excess loading of one of the converters also increases its thermal stress. Therefore, to improve the collective lifetime of the PE converters in a microgrid, it is important to explore the methods to reduce and uniformly distribute the developed thermal stress among all the PE converters.

Usually, the conventional P-ω and Q-V droop laws [13], [14] can distribute the thermal stress caused by T_{jm} to some extent. However, they cannot take care of the effect of stress caused by ΔT_j. Several techniques are proposed to improve the distribution of the thermal stress due to T_{jm} and ΔT_j or in other words the reliability of the PE converters. One of the effective ways to improve reliability is the distribution of active or reactive power or both between the PE converters depending on accumulated damage or junction temperature (T_j). Based on the control architecture, these techniques are categorized as centralized and decentralized control [15]. In [7], an accumulated damage-based centralized optimization technique is proposed, where the power references for all the converters is decided in the central controller based on their accumulated damage values. In another work [8], accumulated damage-dependent virtual impedance emulation technique is proposed. Virtual impedance is emulated to redistribute the current between the converters based on their accumulated damage values. In [9], damage-dependent droop control strategy is proposed. Here, the droop gain is calculated in the central controller and communicated to individual converters

Manuscript received August 26, 2021; revised November 4, 2021; accepted November 19, 2021. Date of publication December 1, 2021; date of current version January 19, 2022. This work was supported in part by the Stability Analysis, Protection and Coordinated Control of Networked Microgrid, Department of Science and Technology (DST), Govt. of India, under Project EE/DST/2018174 and in part by US-India For Smart Distribution System With Storage. Recommended for publication by Associate Editor M. Liserre. *(Corresponding author: Anubrata Das.)*

Anubrata Das and Soumya Ranjan Sahoo are with the Department of Electrical Engineering, Indian Institute of Technology, Kanpur 208016, India (e-mail: anubrata@iitk.ac.in; srsahoo@iitk.ac.in).

Yugal Gupta is with the Bradley Department of Electrical and Computer Engineering, Virginia Tech University, Blacksburg, VA 24060 USA (e-mail: yugal@vt.edu).

Sandeep Anand is with the Department of Electrical Engineering, Indian Institute of Technology, Bombay 400076, India (e-mail: sa@ee.iitb.ac.in).

Color versions of one or more figures in this article are available at https://doi.org/10.1109/TPEL.2021.3131561.

Digital Object Identifier 10.1109/TPEL.2021.3131561

TABLE I
COMPARISON OF DISCUSSED TECHNIQUES

Technique	Applicability for PV	Methodology	Remarks
Raveendran et. al. [10]	Not applicable	Accumulated damage based	Requirement of higher data storage and processing capability of inverter controller
Andresen et. al. [11]	Not applicable		
Peyghami et. al. [12]	Maybe extendable		
Jiang et. al. [14]	Applicable		
Ma et. al. [13]	Applicable	ΔT_{j} based	Central Controller
Wang et. al. [15]	Maybe extendable	T_{j} based	Limited performance in full load
Proposed	Applicable	T_{jm} and ΔT_{j} based	Distributes T_{jm}, reduces ΔT_{j}

to readjust the active power among them depending on their individual damage values. In [11], a reliability improvement technique is proposed by circulating the reactive power between the inverters. The reactive power reference is calculated in the central controller to reduce the magnitude of ΔT_j. This reference reactive power depends on T_j and ΔT_j values of each inverters.

The centralized control architectures are prone to a single point of failure, and they require additional cost to set-up the communication network. To address this, decentralized or communication less lifetime improvement techniques are proposed. The technique in [9] is extended for an ac microgrid application and is implemented in decentralized manner in [10]. In this work, the conventional Q-V droop law is modified to facilitate the distribution of reactive power between the inverters according to their accumulated damage values. In all the accumulated damage-based reliability improvement technique, several electrical and thermal parameters of the converters are measured and stored for a fixed time interval (in the order of months), to calculate the damage. Thus, the damage calculation requires higher data storage and computational ability of the inverter controllers, resulting in higher cost. To address this issue, a temperature-dependent droop law is proposed in [12] and [16]. In these techniques, the active power and reactive power supplied by the inverters are adjusted depending on the junction temperature of the inverters. The key limitation of the technique is that under full load condition these techniques almost reduce to conventional P-ω, and Q-V droop laws.

To fill the gaps in the aforementioned techniques, temperature-dependent droop-based dynamic reactive power sharing (TDDRPS) technique is introduced in this article to distribute the thermal stress uniformly between the inverters with both dispatchable and nondispatchable (PV) energy sources. The proposed TDDRPS technique consists of the following two parts.

1) Distribution of the apparent power in proportion to the nominal rating of the inverter during thermal steady state. During this condition, the proposed technique would ensure the distribution of thermal stress caused by T_{jm}.
2) During thermal transient ($\Delta T_j \neq 0$), the proposed scheme ensures dynamic distribution of reactive power from the inverter with higher value of ΔT_j to lower value of ΔT_j, thereby reducing the value of ΔT_j in all the inverters. Hence, thermal stress due to ΔT_j reduces.

Thus, distribution and reduction of thermal stress due to two primary stressors ensure prolonged operation time of the PE converters-ased microgrid. The design procedure of the droop coefficients for the proposed TDDRPS technique to ensure stable operation of the microgrid is included in this article. Furthermore, the proposed technique is validated through simulation and experimentally in a laboratory grade microgrid prototype. Qualitative comparison with the existing techniques is given in Table I .

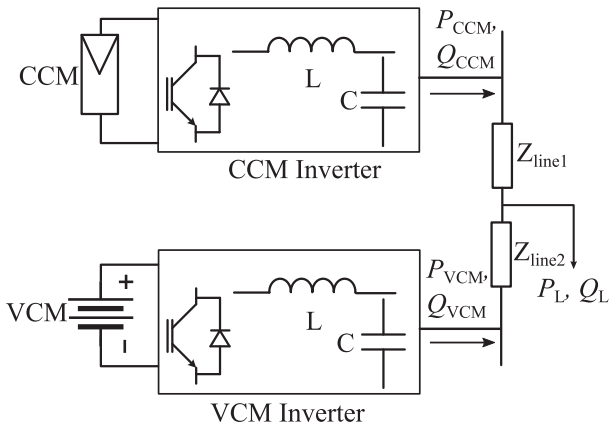

Fig. 1. Two inverter microgrid system including CCM (PV) and VCM (battery) inverter.

The rest of this article is organized as follows. The brief methodology of reactive power re-routing strategy and consequently the proposed TDDRPS technique are presented in Section II. In Section III, the small signal modeling of the inverter with the proposed controller is carried out to investigate the stability. The proposed technique is verified through simulation and experimentation and the results are included in Section IV. Finally, Section V concludes the article.

II. PROBLEM IDENTIFICATION AND PROPOSED TECHNIQUE

This section investigates the key reasons behind reduced lifetime of PE converters in a microgrid in the presence of PV. The proposed TDDRPS technique to improve the collective lifetime of the PE converters is discussed afterward. A PV and battery inverter-based microgrid system are shown in Fig. 1, for this discussion. The same discussion can be extended for a generalized microgrid structure with more number of PV and battery inverters.

A. Lifetime Model of PE Device

Junction temperature (T_{jm} and ΔT_j) causes contraction-expansion cycle of bond wire and solder joints in the PE device like IGBT resulting in development of fatigue in bond wire and solder joints. Accumulation of fatigue leads to wire out of bond

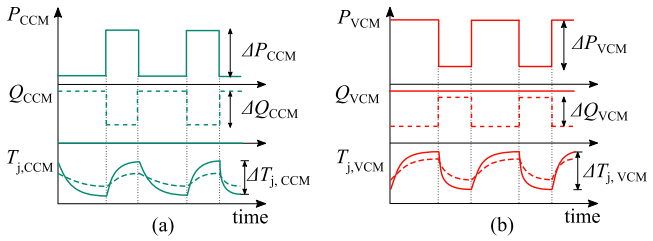

Fig. 2. Active power, reactive power, and junction temperature characteristics of CCM and VCM inverter. (a) Active power delivered by the CCM inverter (P_{CCM}), reactive power delivered by the CCM inverter (Q_{CCM}), and junction temperature of the CCM inverter ($T_{\mathrm{j,CCM}}$). (b) Active power delivered by the VCM inverter (P_{VCM}), reactive power delivered by the VCM inverter (Q_{VCM}), and junction temperature of the VCM inverter ($T_{\mathrm{j,VCM}}$). Traces: Solid lines—without reactive power rerouting technique. Dotted lines—with reactive power rerouting technique.

wire and cracks in solder joints, thus leading to failure of IGBT. The effect of T_{jm} and ΔT_j on the lifetime of the IGBT as given in [7] is

$$N_f = a_1[\Delta(T_j)]^{a_2} \times e^{\frac{a_3}{(T_{jm}+273)}} \tag{1}$$

where N_f is the number of cycle of operation of IGBT before the failure. The values of a_1, a_2, and a_3 are the device-dependent parameters. In general, the value of the a_2 varies from -3 to -5, which makes ΔT_j to be more dominant than T_{jm} affecting the lifetime of the IGBT. In the next section, the reasons for variation in T_{jm} and ΔT_j are discussed.

B. Effect of Intermittent Generation and Load Profile

Conventionally, the PV inverter is operated in current controlled mode (CCM) to extract maximum power under any environmental condition. Similarly, the load reactive power (Q_{L}) is shared by the battery inverters operating in voltage control mode (VCM). The power loss in CCM inverter varies with the active power generation (P_{CCM}), which in turn results variation in junction temperature ($T_{\mathrm{j,CCM}}$) as shown in Fig. 2(a) in solid line. The battery inverter supplies the rest of load active power demand ($P_{\mathrm{L}} - P_{\mathrm{CCM}}$). Therefore, variation in P_{CCM}, also results in the change in the power delivered by the VCM inverter (P_{VCM}) as shown in Fig. 2(b) in solid line, which in turn results in varying junction temperature profile ($T_{\mathrm{j,VCM}}$) of VCM inverter, shown in Fig. 2(b) in solid line. Therefore, frequent variation in the P_{CCM} (generally in the order of minutes), which is common in tropical region like India, result in low frequency oscillations in $T_{\mathrm{j,CCM}}$ and $T_{\mathrm{j,VCM}}$.

Also, with the proliferation of electric vehicles (EV), the load profile becomes stochastic in nature. Therefore, with the variation in load active (P_{L}), and reactive (Q_{L}) power demand, $T_{\mathrm{j,CCM}}$ and $T_{\mathrm{j,VCM}}$ also vary. This varying nature of $T_{\mathrm{j,CCM}}$ and $T_{\mathrm{j,VCM}}$ due to intermittent source and load profile reduces the lifetime of the VCM and CCM inverters. In the following section, the motivation behind temperature-dependent reactive power sharing is discussed.

C. Motivation of Temperature-Dependent Reactive Power Sharing

In this article, temperature-dependent reactive power sharing approach is adopted. In this approach, the magnitude of the reactive power shared by the inverters is dynamically decided depending on the magnitude of ΔT_j. For example, the reactive power shared by the inverter should be increased whenever negative ΔT_j appears at the junction of the inverter and vice versa. In Fig. 2(a) and (b), solid lines represent a case whenever temperature-dependent power sharing is not used. As, shown in Fig. 2(a), in case of an increase in P_{CCM} a large value of $\Delta T_{\mathrm{j,CCM}}$ occurs. So, in this duration if Q_{CCM} is reduced depending on the magnitude of $\Delta T_{\mathrm{j,CCM}}$, a reduced value of $\Delta T_{\mathrm{j,CCM}}$ is expected to achieve which is shown in dotted line. The same explanation can be extended for VCM inverter. In the following section, the proposed technique is discussed to facilitate temperature-dependent power sharing and to obtain a T_{jm} and ΔT_j behavior as shown in Fig. 2(a) and (b) in dotted lines.

D. Proposed TDDRPS Technique

The proposed technique 1) maintains uniform distribution of T_{jm} between the PV and the battery inverter, 2) reduces ΔT_j in both the PV and the battery inverters. The general structure of the TDDRPS technique is

$$V_i = V_{\mathrm{nom}} - m_i S_{i,\mathrm{del}} - n_i \alpha_i \Delta T_{j,i} \tag{2}$$

where subscript i denotes the ith inverter, V_{nom} and V_i are the nominal voltage and the peak value of the inverter voltage, respectively, $S_{i,\mathrm{del}}$ is the average value of the delivered apparent power, $\Delta T_{j,i}$ is the magnitude of junction temperature ripple in the inverter. Depending on the mode of operation of the inverter (CCM or VCM) α_i is either the average value of delivered apparent power ($S_{i,\mathrm{del}}$) or reactive power ($Q_{i,\mathrm{del}}$). m_i and n_i are the droop coefficients of the proposed method. The expression for m_i is

$$m_i = \frac{\Delta V}{S_{i,\mathrm{nom}}} \tag{3}$$

where ΔV is the allowable voltage deviation from V_{nom}, and $S_{i,\mathrm{nom}}$ is the nominal rating of the ith inverter. Therefore, in the thermal steady state ($\Delta T_{j,i} = 0$), the following condition is satisfied:

$$m_1 S_{1,\mathrm{del}} = m_2 S_{2,\mathrm{del}} = \cdots = m_i S_{i,\mathrm{del}}. \tag{4}$$

From (4), the proposed control ensures the sharing of the apparent power proportional to their rating during thermal steady state. As, the current in the inverter depends on the $S_{i,\mathrm{del}}$ delivered by the inverter, sharing of apparent power ensures uniform distribution of mean junction temperature (T_{jm}) among the inverters during thermal steady state ($\Delta T_j = 0$).

The expression for n_i is

$$n_i = \frac{\Delta V}{\alpha_{i,\mathrm{nom}} \Delta T_{\mathrm{j,max}}} \tag{5}$$

$\alpha_{\mathrm{i,nom}}$ can be either $S_{i,\mathrm{nom}}$ or $Q_{i,\mathrm{nom}}$ depending on whether the inverter is operating at CCM or VCM, respectively. $\Delta T_{\mathrm{j,max}}$ is the maximum allowable junction temperature swing value. Change in source or load power results in occurrence of $\Delta T_{j,i}$ at the junction of the inverter. Therefore, in this condition, the term $n_i\alpha_i\Delta T_{j,i}$ in (2) becomes nonzero. Thus, during thermal transients, the $\Delta T_{j,i}$ dependent term further modifies the magnitude of V_i. Hence, depending on the magnitude of $\Delta T_{j,i}$, the proposed technique is expected to redistribute the reactive power between the inverters, such that the magnitude of $\Delta T_{j,i}$ in the inverter reduces.

In the microgrid, inverters operate either in CCM or in VCM, the implementation of the proposed TDDRPS technique in (2) would be different for CCM and VCM inverters.

1) For CCM Inverter: It is worth mentioning that the CCM inverter does not absorb reactive power during the thermal transient ($\Delta T_j \neq 0$) for the following reasons.

1) In case of negative ΔT_j, the CCM inverter increases the magnitude of $Q_{i,\mathrm{del}}$, and thus, reduces the magnitude of the ΔT_j.
2) In case of positive ΔT_j, the CCM inverter reduces the magnitude of $Q_{i,del}$, and thus, reduces the magnitude of ΔT_j.

Thus, under any operating conditions when $\Delta T_j \neq 0$, $Q_{i,del}$ never becomes negative. Hence, the term "α_i" in (2) does not have directional property for CCM inverter. So, α_i in (2) is set to $S_{i,\mathrm{del}}$. Thus, the TDDRPS technique for CCM inverter becomes

$$V_i = V_{\mathrm{nom}} - m_i S_{i,\mathrm{del}} - n_i S_{i,\mathrm{del}} \Delta T_{j,i}. \tag{6}$$

From (6), the reactive or q-axis reference current ($i^*_{q,i}$) is calculated as follows:

$$S_{i,\mathrm{del}} = \frac{V_{\mathrm{nom}} - V_i}{m_i + n_i \Delta T_{j,i}}. \tag{7}$$

From (7), $Q_{i,\mathrm{del}}$ is calculated as

$$Q_{i,\mathrm{del}} = \sqrt{\left[\left(\frac{V_{\mathrm{nom}} - V_i}{m_i + n_i \Delta T_{j,i}}\right)^2 - P^2_{i,\mathrm{del}}\right]} \tag{8}$$

where $P_{i,\mathrm{del}}$ is the active power delivered by the CCM inverter. From (8), $i^*_{q,i}$ is calculated from $Q_{i,\mathrm{del}}$ as

$$i^*_{q,i} = \frac{1}{V_{d,i}}\left(V_{q,i} i_{d,i} - \frac{2}{3} Q_{i,\mathrm{del}}\right) \tag{9}$$

where $V_{d,i}$, and $V_{q,i}$ are the d-axis and q-axis components of the inverter terminal voltage, respectively.

2) For VCM Inverter: The directional property of α_i in (2) is required for the VCM inverter for the following reason.

1) In case ΔT_j of VCM inverter is negative, the VCM inverter can either absorb the reactive power or increase the magnitude of delivered reactive power depending on the level of reactive power injection by the CCM inverter

Therefore, under some operating conditions, $Q_{i,\mathrm{del}}$ for VCM inverter can be negative. Hence, to facilitate the directional property in (2), α_i is made equal to $Q_{i,\mathrm{del}}$ for the VCM inverter. Thus, the TDDRPS technique for VCM inverter becomes

$$V_i = V_{\mathrm{nom}} - m_i S_{i,\mathrm{del}} - n_i Q_{i,\mathrm{del}} \Delta T_{j,i}. \tag{10}$$

E. Overall Control Structure

The control diagram for the ith VCM inverter is shown in Fig. 3(a). The frequency of the microgrid (ω) is determined with conventional $P-\omega$ droop law. The peak value of the inverter voltage (V_i) is calculated through (10). As shown in Fig. 3(a), V_i and ω are fed to the voltage loop of the inverter to generate the gate signal.

The control diagram for the ith CCM inverter is shown in Fig. 3(b). The reference PV voltage ($\mathrm{v}^*_{\mathrm{pv}}$) is determined using maximum power point tracking (MPPT) algorithm. The q-axis reference current ($i^*_{q,i}$) is calculated through (6)–(9). As shown in Fig. 3(b), $\mathrm{v}^*_{\mathrm{pv,i}}$ and $i^*_{q,i}$ is fed to the voltage and current loop, to generate the gate signal for the CCM inverter.

III. Mathematical Analysis

In this section, the stability analysis of the proposed control technique is carried out.

A. For CCM Inverter

Proposed TDDRPS technique for the CCM inverter is given in (6). In practice, measured $S_{i,\mathrm{del}}$ is passed through low-pass filters (LPF) before using in (6). Therefore, incorporating the dynamics of LPF, (6) becomes

$$V_i = V_{\mathrm{nom}} - m_i \frac{\omega_{lf}}{s+\omega_{lf}} S_{i,\mathrm{del}} - n_i \frac{\omega_{lf}}{s+\omega_{lf}} S_{i,\mathrm{del}} \Delta T_{j,i} \tag{11}$$

where ω_{lf} is the cutoff frequency of the LPF. $\Delta T_{j,i}$ in (11) is obtained by passing $T_{j,i}$ through a high-pass filter (HPF). Furthermore, a separate LPF whose cutoff frequency is similar to the LPF of $S_{i,\mathrm{del}}$ is used while estimating $T_{j,i}$. Therefore, incorporating the dynamics of these, (11) becomes

$$V_i = V_{\mathrm{nom}} - m_i \frac{\omega_{lf}}{s+\omega_{lf}} S_{i,\mathrm{del}} - n_i \frac{\omega_{lf}}{s+\omega_{lf}} S_{i,\mathrm{del}} \frac{s}{s+\omega_c} \frac{\omega'_{lf}}{s+\omega'_{lf}} T_{j,i} \tag{12}$$

where ω_c is the passband frequency of HPF and ω'_{lf} is the cutoff frequency of LPF for estimating $T_{j,i}$. It is worth noting that in practice a very low value of ω_c is used to extract even very low frequency component of ΔT_j. Therefore, in practice $\omega_c \ll \omega_{lf}$, and ω'_{lf}. Hence, the dynamics in (12) is approximated to

$$V_i = V_{\mathrm{nom}} - m_i S_{i,\mathrm{del}} - n_i S_{i,\mathrm{del}} \frac{s}{s+\omega_c} T_{j,i}. \tag{13}$$

Rearranging (13) gives

$$n_i S_{i,\mathrm{del}} \frac{s}{s+\omega_c} T_{j,i} = V_{\mathrm{nom}} - V_i - m_i S_{i,\mathrm{del}} \tag{14}$$

$$\Longrightarrow \frac{y}{u} = \frac{s}{s+\omega_c} \tag{15}$$

where $y = V_{\mathrm{nom}} - V_i - m_i S_{i,\mathrm{del}}$, and $u = n_i S_{i,\mathrm{del}} T_{j,i}$. Rearranging (15)

$$\frac{y}{u} = 1 - \frac{\omega_c}{s+\omega_c} \tag{16}$$

$$y = u - x \tag{17}$$

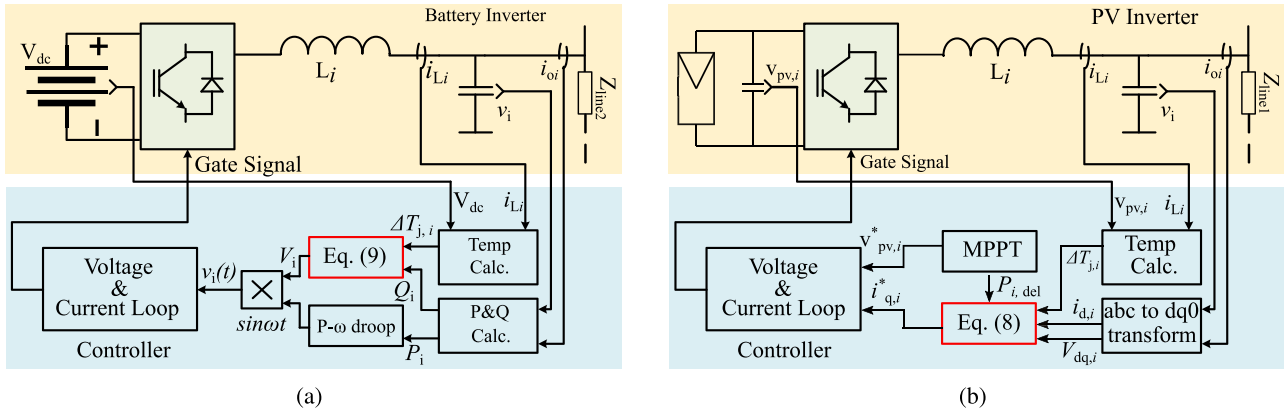

(a) (b)

Fig. 3. Control block diagram of (a) VCM inverter and (b) CCM inverter.

where $x = u\dfrac{\omega_c}{s+\omega_c}$. Therefore

$$\dot{x} = -\omega_c x + \omega_c u \tag{18}$$

$$y = -x + u. \tag{19}$$

Now, for all practical applications, since ω_c is a positive quantity, the eigenvalues of (18) always lie in the negative half of the s-plane. Therefore, for bounded value of $n_i S_{i,\text{del}} T_{j,i}$, the system is always stable with the proposed controller.

B. For VCM Inverter

The proposed TDDRPS technique for the VCM inverter is given in (10). Approaching with the same philosophy like in CCM, (10) becomes

$$V_i = V_{\text{nom}} - m_i S_{i,\text{del}} - n_i Q_{i,\text{del}} \frac{s}{s+\omega_c} T_{j,i}. \tag{20}$$

Rearranging (20)

$$n_i Q_{i,\text{del}} \frac{s}{s+\omega_c} T_{j,i} = V_{\text{nom}} - V_i - m_i S_{i,\text{del}} \tag{21}$$

$$\Longrightarrow \frac{g}{h} = \frac{s}{s+\omega_c} \tag{22}$$

where $g = V_{\text{nom}} - V_i - m_i S_{i,\text{del}}$, and $h = n_i Q_i T_{j,i}$. Following the steps used for CCM inverter

$$\dot{x} = -\omega_c x + \omega_c h \tag{23}$$

$$g = -x + h. \tag{24}$$

Here, also ω_c is a positive quantity, therefore, the eigenvalues of (23) always lie in the negative half of the s-plane. Therefore, for bounded value of $n_i Q_{i,\text{del}} T_{j,i}$, the system is always stable with the proposed controller.

IV. Results

A. Simulation Study

The proposed technique is validated through a detailed simulation study in MATLAB on two 10 kVA inverters-based microgrid system as shown in Fig. 1. The parameters of the system is given in Table II. To validate the operating principle of the proposed TDDRPS technique, a step change in load power and CCM power are considered at first. Furthermore, to investigate the effectiveness of the proposed technique for practical scenario, a mission profile of CCM (PV) active power is considered.

TABLE II
Specifications of the Simulated System

Symbol	Parameter	Value
$S_{\text{CCM}}, S_{\text{VCM}}$	Rating of inverter	10 kVA
–	Load (Pre-disturbance)	P_L=6 kW, Q_L=5 kVAr
f_{nom}	Nominal frequency	50 Hz
V_{nom}	Nominal phase voltage	230 V (RMS)
f_{s}	Switching frequency	10 kHz
Z_{line1}	Line impedance 1	r=0.2 $m\Omega$, L=5.3 μH
Z_{line2}	Line impedance 2	r=0.1 $m\Omega$, L=2.65 μH

1) Step Change in CCM (PV) Active Power: In this case, the CCM active power is increased in step by 50 % at 12 min and restored to the initial power level at 13 min. For this case, the TDDRPS technique is first compared with the conventional or UPF operation of CCM inverter.

1) Conventional operation: In this case, the CCM inverter operates at maximum power point and supplies zero reactive power. Consequently the VCM inverter supplies rest of P_{L} and Q_{L} demand as shown in Fig. 4(a) and (b), respectively. With the increase in P_{CCM}, $T_{\text{j,CCM}}$ increases and consequently $T_{\text{j,VCM}}$ decreases as shown in Fig. 4(c). $T_{\text{j,CCM}}$, $T_{\text{j,VCM}}$, and ΔT_j values for the CCM and VCM inverter are given in Table III.

2) TDDRPS technique: During $\Delta T_j = 0$, proposed TDDRPS technique ensures sharing of apparent power in proportion to the rating of the CCM and the VCM inverter. The active and reactive power profile of CCM and VCM inverters are shown in Fig. 4(d) and (e), respectively. As a result, the T_j of the CCM and VCM inverters become almost equal as shown in Fig. 5(f). During the step change in PV power, due to ΔT_j based dynamic reactive power sharing, ΔT_j values of both CCM and VCM inverter

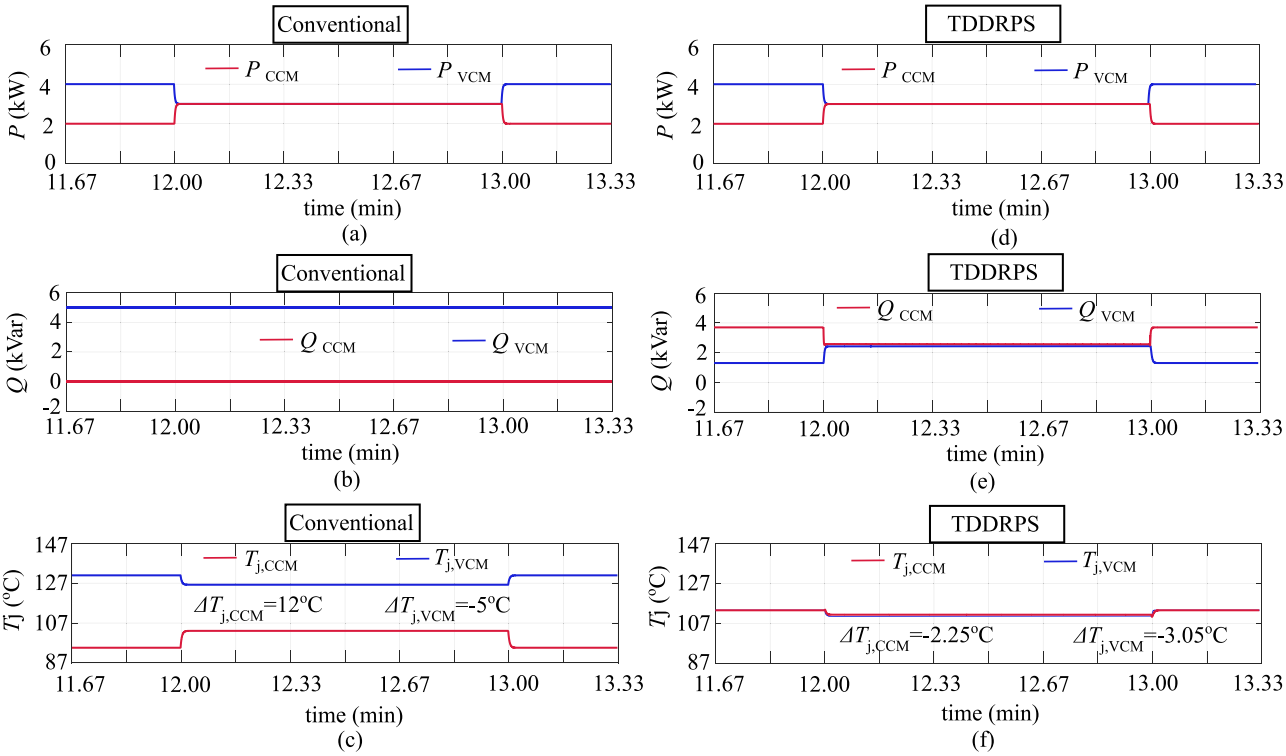

Fig. 4. Simulation results for step change in P_{CCM}. (a) Active power profile for CCM and VCM inverter for conventional operation (2 kW/div). (b) Reactive power profile for CCM and VCM inverter for conventional operation (2kVar/div). (c) Junction temperature profile for CCM and VCM inverter with the conventional operation (20 °C/div). (d) Active power profile for CCM and VCM inverter for TDDRPS operation (2 kW/div). (e) Reactive power profile for CCM and VCM inverter with TDDRPS technique (2kVar/div). (f) Junction temperature profile for CCM and VCM inverter with TDDRPS technique (20 °C/div).

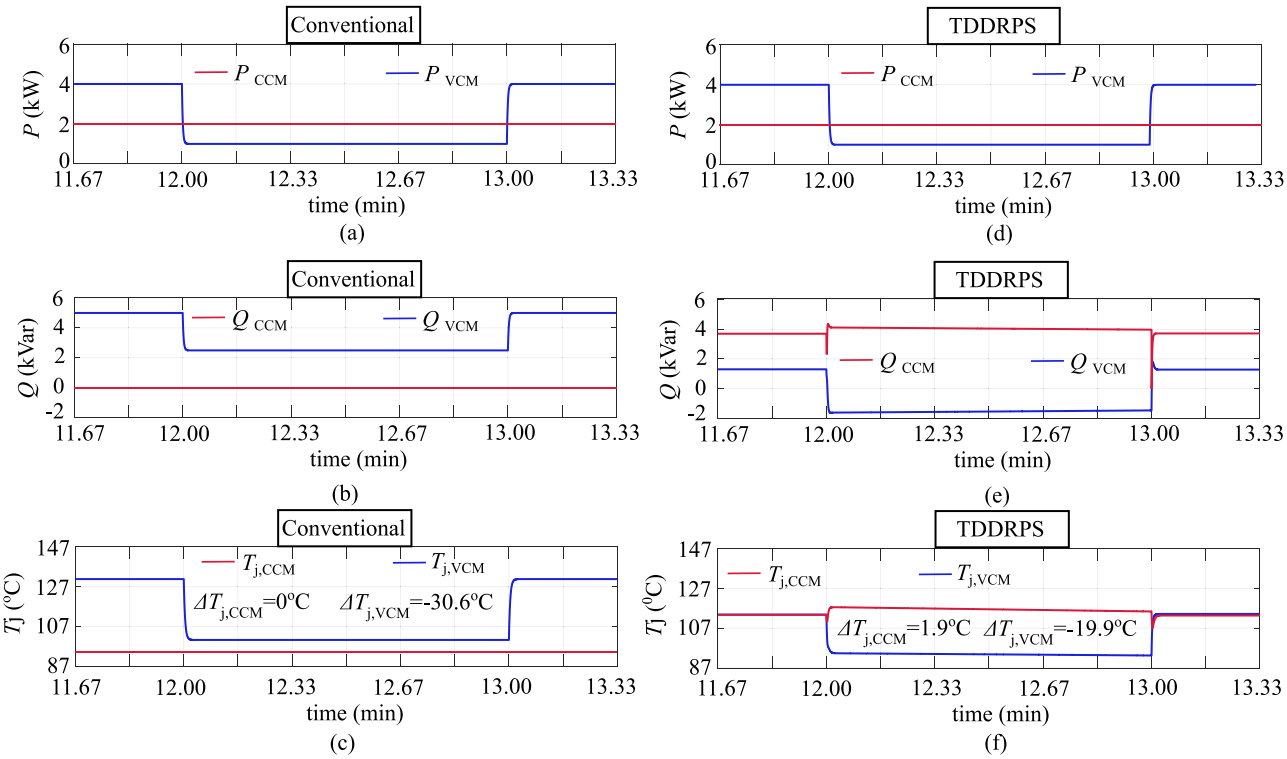

Fig. 5. Simulation results for step change in load. (a) Active power profile for CCM and VCM inverter for the conventional operation (2 kW/div). (b) Reactive power profile for CCM and VCM inverter for the conventional operation (2kVar/div). (c) Junction temperature profile for CCM and VCM inverter with the conventional operation (20 °C/div). (d) Active power profile for CCM and VCM inverter for TDDRPS operation (2 kW/div). (e) Reactive power profile for CCM and VCM inverter with TDDRPS technique (2kVar/div). (f) Junction temperature profile for CCM and VCM inverter with TDDRPS technique (20 °C/div).

TABLE III
PERFORMANCE COMPARISON

Disturbances	Inv.	Condition	Conventional		TDDRPS	
			T_j	ΔT_j	T_j	ΔT_j
Change in CCM Active Power	CCM	BT	93	12	113.65	-2.25
		AT	105		111.4	
	VCM	BT	131	-5	113.75	-3.05
		AT	126		110.7	
Change in Load Power Demand	CCM	BT	94.62	0	111.6	1.9
		AT	94.62		113.5	
	VCM	BT	131	-30.6	112	-19.9
		AT	100.4		92.1	

BT= Before Transient; AT= After Transient; T_j and ΔT_j values are in °C

decrease as compared with the conventional operation, shown in Fig. 4(f). The T_{jm} and ΔT_j values with TDDRPS technique are listed in Table III

2) Step Change in Load Power Demand: In this case, both the $P_{\rm L}$ and $Q_{\rm L}$ are decreased by 50% at 12 min and restored to the initial power level at 13 min. In this case also, the TDDRPS technique is compared with UPF operation of CCM inverter.

1) Conventional operation: As shown in Fig. 5(a) and (b), $P_{\rm CCM}$ and $Q_{\rm CCM}$ remain constant during the change in load. Consequently $P_{\rm VCM}$ and $Q_{\rm VCM}$ change to maintain the $P_{\rm L}$ and $Q_{\rm L}$ demand. Thus, as shown in Fig. 5(c), during the load switching $\Delta T_{\rm j,VCM}$ becomes -30.6 °C while $\Delta T_{\rm j,CCM}$ remains at 0 °C. The T_{jm} and ΔT_j values for this case are given in Table III.

2) TDDRPS technique: As shown in Fig. 5(e), the $Q_{\rm CCM}$ value is adjusted such that the inverters share the apparent power in proportion to their ratings. Therefore, as shown in Fig. 5(f), the T_j values for VCM and CCM inverters are very close to each other compared to the conventional operation. At the time of load change, due to ΔT_j dependent reactive power sharing, the ΔT_j value of the VCM inverter becomes -19.9 °C and for the CCM inverter ΔT_j becomes 1.9 °C. Thus, the cumulative damage of the system decreases with this technique as compared to conventional operation. In Table III, the T_{jm} and ΔT_j values of both CCM and VCM inverters are listed.

3) Mission Profile-Based Comparison of TDDRPS With Other Techniques: The proposed TDDRPS technique tested for a weekly mission profile of CCM (PV) active power and ambient temperature ($T_{\rm a}$) and compared with the conventional operation, QV droop, and lifetime oriented droop control [12]. The $P_{\rm CCM}$ and $T_{\rm a}$ data are collected from Solar Energy Research Enclave (SERE), IIT Kanpur, India (26.4499° N, 80.3319° E) for a week in August 2018. In Fig. 6(a) and (b), $P_{\rm CCM}$ and $T_{\rm a}$ are shown for a particular day out of that week. To analyze the performance of the TDDRPS technique, the normalized accumulated damage is calculated for TDDRPS technique and compared with the aforementioned techniques. For this article, the load power demand ($P_{\rm L}$ and $Q_{\rm L}$) is set to 3 kW and 2 kVar.

The accumulated damage is calculated for all these techniques using rainflow analysis [17] and miner's rule [18]. To normalize the accumulated damage in the inverters, a lifetime of eight years (i.e., accumulated damage is 100%) for the VCM inverter with

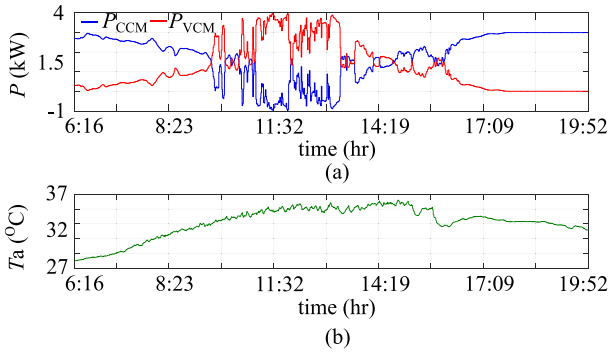

Fig. 6. Daily mission profile. (a) Active power profile (1 kW/div). (b) Ambient temperature profile (2°C/div).

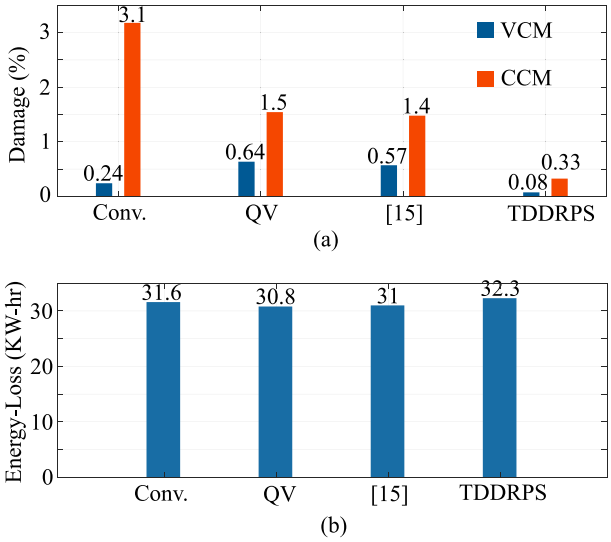

Fig. 7. Comparison of techniques in terms of (a) normalized accumulated damage (0.5 %/div) and (b) energy loss (5 kW-hr/div).

conventional operation is assumed. Moreover, as the accumulated damage also influences the energy loss, these techniques are also compared in terms of energy loss in CCM and VCM inverters over the considered week.

1) Damage comparison: The normalized accumulated damage values (in percentage) are presented in Fig. 7(a). The difference in the accumulated damage values in the VCM and CCM inverters with the conventional operation is highest as compared to all the other techniques. This is because, in this case, the $Q_{\rm CCM}$ is zero. It is observed from Fig. 7(a), that the difference in the accumulated damage values is minimum with the proposed TDDRPS technique as compared to the other techniques. This validates that the proposed technique uniformly (or almost uniformly) distributes thermal stress between the inverters as compared to the other techniques. Furthermore, the overall reliability of the microgrid can be related to the maximum of damage values occurred in CCM and VCM inverters. From Fig. 7(a) with the proposed TDDRPS technique, the maximum value of damage decreases by a factor of

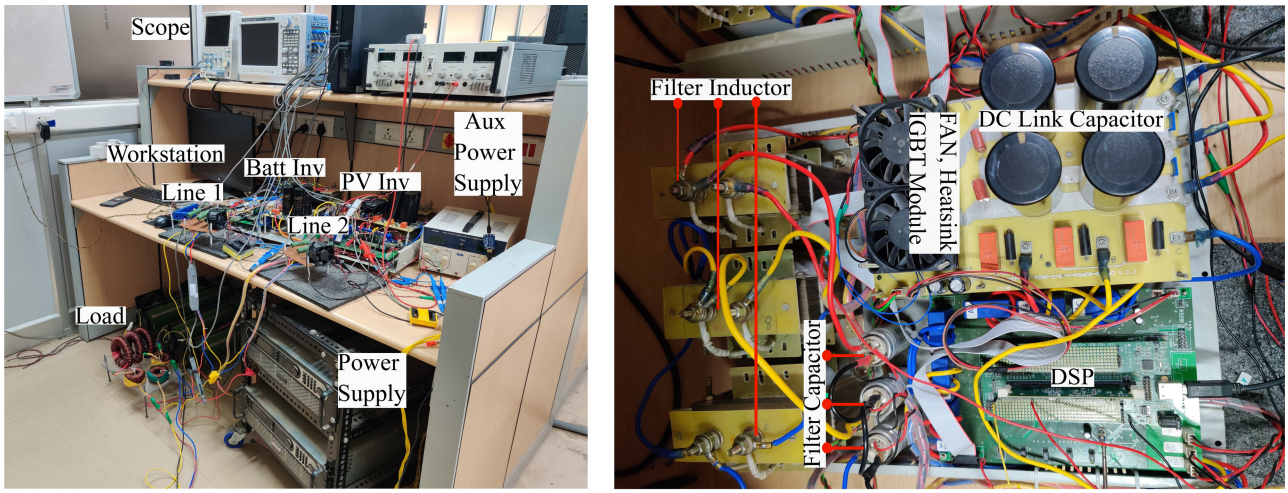

(a) (b)

Fig. 8. Developed experimental prototype. (a) Two inverter ac microgrid system. (b) Details of the single inverter.

9.39, 4.54, and 4.24 as compared with the conventional operation, QV droop, and [12] respectively.

2) *Energy loss:* A tradeoff exists between the energy loss and the accumulated damage in the inverter [19]. Therefore, it is important to compare all the techniques in terms of the energy loss. In this case, the total energy loss for the duration of the considered week are calculated for all the techniques and shown in Fig. 7(b). It is found that with the TDDRPS technique the energy loss increases by a factor of 1.02, 1.05, and 1.04 as compared with the conventional operation, QV droop, and [12], respectively.

Therefore, from Fig. 7(a) and (b), it can be concluded that with the TDDRPS technique the effective lifetime of the microgrid improves significantly as compared with other techniques while the increase in the energy loss is not that significant compared to decrease in accumulated damage value.

B. Experimental Study

The proposed technique is experimentally validated in a scaled down laboratory prototype of a 3-ϕ 4-wire microgrid system as shown in Fig. 8. This setup follows the schematic shown in Fig. 1. In the experimental setup, each of the inverter is realized using FNA22512 A IGBT module (ON semiconductor make). TMS230F28335 Delphino controllers (Texas Instruments make) are used in each of the inverter to implement the control loops. A combination of resistance and inductance is used as a central load to the inverter system. The parameters for experimental prototype are listed in Table IV. For the experimental studies, the thermo-electric model of IGBT and diode is used to estimate the junction temperature [20]. ΔT_j is calculated by passing T_j through a high-pass filter.

The TDDRPS technique is compared with the conventional operation of CCM inverter for experimental study. Following two cases are considered for the comparison:

1) step change in CCM active power;
2) step change in load active and reactive power demand.

TABLE IV
SPECIFICATION FOR EXPERIMENTAL PROTOTYPE

Symbol	Parameter	Value
S_{CCM}, S_{VCM}	Rating of inverter	500 VA
P_L, Q_L	Load (Pre-disturbance)	P_L=310 W, Q_L=140 VAr
f_{nom}	Nominal frequency	50 Hz
V_{nom}	Nominal phase voltage	21.21 V (RMS)
f_s	Switching frequency	10 kHz
Z_{line1}	Line impedance 1	r=0.25 $m\Omega$, L=120 μH
Z_{line2}	Line impedance 2	r=0.5 $m\Omega$, L=230 μH

In practice, the source and the load power change in a smooth ramp like manner, but here they are deliberately considered to be in step to clearly demonstrate the advantage of the proposed scheme. In all the cases, a step change is done at 900 s which is restored to the initial value at 990 s. The short interval of 90 s is considered so that the junction temperature does not reach to its steady state value in this duration.

1) Change in CCM Active Power (P_{CCM}): In this case, P_{CCM} is decreased by 65.56% in step at 900 s, and restored to its initial operating condition at 990 s. The detailed voltage, current, and power waveforms with TDDRPS technique is shown in Fig. 9(a) for reference.

1) *Conventional operation:* In this case, the CCM inverter supplies only maximum available active power, while the VCM inverter supplies the rest of the P_{L} and total Q_{L} demand. The initial temperatures of CCM and VCM inverters are given in Table V. After the change in P_{CCM}, $T_{\text{j,CCM}}$ decreases as shown in Fig. 9(b). As P_{CCM} decreases, P_{VCM} increases to maintain the P_L as shown in Fig. 9(a). Hence, in this duration, $T_{\text{j,VCM}}$ increases as shown in Fig. 9(b). $T_{\text{j,CCM}}$ and $T_{\text{j,VCM}}$ after the change in the active power and the ΔT_j values for the CCM and VCM inverters are given in Table V.

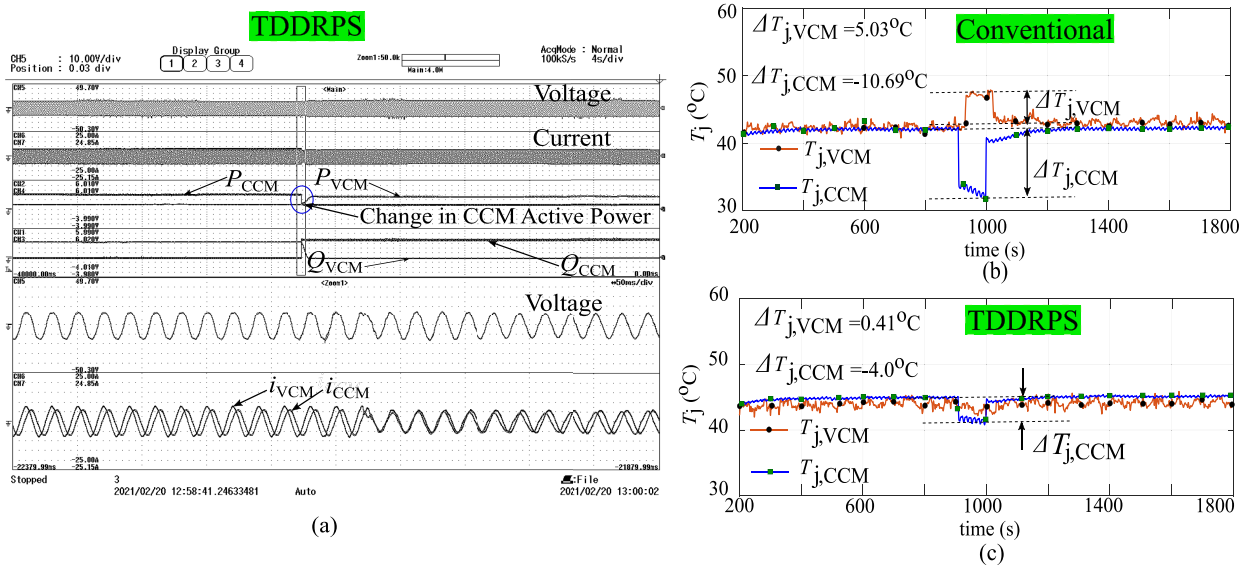

Fig. 9. Comparison of thermal distribution performance with change in CCM active power. (a) Voltage (10 V/div), current (5 A/div), active power (60 W/div), reactive power (34 VAr/div) for the proposed TDDRPS technique. (b) Junction temperature (T_j) (10 °C/div) for the conventional operation. (c) Junction temperature (T_j) (10 °C/div) for TDDRPS technique.

TABLE V
PERFORMANCE COMPARISON

Disturbances	Inv.	Condition	Conventional P	Q	T_j	ΔT_j	TDDRPS P	Q	T_j	ΔT_j
Change in CCM Active Power	CCM	BT	185.27	0	42.38	-10.7	181.26	11.54	44.97	-4.0
		AT	68.39	0	31.68		66.46	158.26	40.97	
	VCM	BT	68.91	150.5	42.36	5.03	71.45	142.48	43.83	0.41
		AT	175.96	142.5	47.39		169.21	-9.26	44.24	
Change in Load Power Demand	CCM	BT	73.9	0	33.33	-0.22	68.97	128.7	41.69	-2.08
		AT	74.09	0	33.11		72.08	128.6	39.63	
	VCM	BT	207.58	152.9	49.45	-11.38	203.34	27.63	45.84	-6.28
		AT	86.91	83.9	38.07		78.54	-40.33	39.56	

BT= Before transient; AT= After transient; P &amp; Q values are in W and VAR, respectively; T_j and ΔT_j values are in °C.

2) *TDDRPS technique:* TDDRPS technique is implemented to further improve the thermal stress sharing. Prior to any change in $P_{\rm CCM}$, $T_{\rm j,CCM}$, and $T_{\rm j,VCM}$ with this technique are shown in Fig. 9(c). From (2) and (6), in the absence of any swing in ΔT_j, the TDDRPS technique ensures the sharing of apparent power in proportion to the rating of the inverters. The T_{jm} and ΔT_j values before and after the step change in $P_{\rm CCM}$ are given in Table V. Thus, with the proposed TDDRPS technique, as given in Table V, because of temperature-based dynamic reactive power sharing between the inverters, the ΔT_j values are reduced by a factor of 2.67 and 12.26 for CCM and VCM inverters, respectively, compared with the conventional operation.

2) *Change in Load Power:* In this case, $P_{\rm L}$ and $Q_{\rm L}$ are decreased by 49.33%, and 45.12%, respectively, at 900 s and restored to initial operating condition at 990 s. The detailed waveforms of current voltage and inverter power are shown in Fig. 10(a) with TDDRPS technique.

1) *Conventional operation:* Initial $T_{\rm j,CCM}$ and $T_{\rm j,VCM}$ are shown in Fig. 10(b). From the value of $T_{\rm j,CCM}$, and $T_{\rm j,VCM}$ given in Table V, the difference in T_{jm} values is 16.12 °C. After decreasing $P_{\rm L}$, and $Q_{\rm L}$, $T_{\rm j,CCM}$, and $T_{\rm j,VCM}$ settle to 33.11 °C and 38.07 °C, respectively, given in Table V. As already explained, $T_{\rm j,CCM}$ before and after the load change remains almost same. Therefore, to maintain the load power, the active, and reactive power catered by the VCM inverter reduces, resulting in large value of $\Delta T_{\rm j,VCM}$ compared to $\Delta T_{\rm j,CCM}$, as given in Table V.

2) *TDDRPS technique:* With the proposed TDDRPS technique, from the initial T_{jm} values as given in Table V, the difference in the junction temperatures is 4.15 °C. Thus, due to apparent power sharing, the difference in the T_j values reduces. The T_j profile for the CCM and the VCM inverters are shown in Fig. 10(c). After the change in load, to reduce the ΔT_j values in both the inverters, the reactive power is adjusted in such a way that, it circulates between the two inverters. Thus, the reactive power delivered by the VCM inverter is negative as given in Table V. $T_{\rm j,CCM}$, and $T_{\rm j,VCM}$ values after the change in load are given in Table V. With the TDDRPS technique the ΔT_j value for CCM inverter is increased by a factor of 9.45 and for VCM inverter it decreases by a factor of 1.81 as compared with

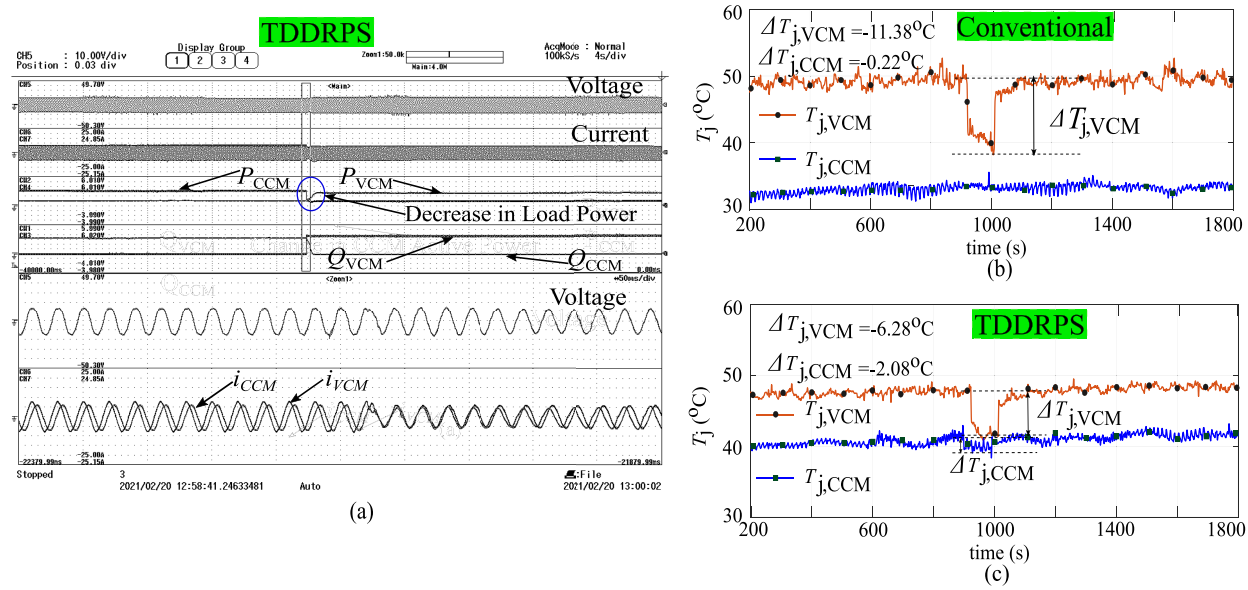

Fig. 10. Comparison of thermal distribution performance with decrease in load. (a) Voltage (10 V/div), current (5 A/div), active power (60 W/div), reactive power (34 VAr/div) for proposed TDDRPS technique. (b) Junction temperature (T_j) (10 °C/div) for the conventional operation. (c) Junction temperature (T_j) (10 °C/div) for TDDRPS technique.

the conventional operation. It is worth mentioning that, as $P_{\rm CCM}$ does not change with the change in load, thus the ΔT_j value is lower in case of conventional operation as compared with the proposed TDDRPS technique.

Hence, from the results it can be concluded that with the proposed technique, the thermal stress due to ΔT_j on the IGBT switches reduces. Furthermore, in the steady state, as the proposed technique ensures sharing of apparent power in proportion to the nominal rating of the inverters, therefore in the thermal steady-state condition the mean junction temperature is also uniformly distributed between the inverters.

V. Conclusion

A temperature droop-based dynamic apparent power sharing technique is proposed to improve the lifetime of a nondispatchable energy sources-based microgrid system. The proposed technique reduces the thermal stress due to mean junction temperature and junction temperature swing. The droop law-based structure of the proposed technique enables decentralized implementation. Hence, no additional communication infrastructure is required. The stability analysis of the proposed control is carried out. The proposed technique is validated for step change in CCM and the load power. Furthermore, the proposed TDDRPS technique is compared with other relevant techniques for a weekly mission profile of CCM (PV) active power. It is observed that with the TDDRPS technique the maximum of damage values in CCM and VCM converters reduces significantly compared to other techniques. A scaled down laboratory prototype is developed to validate the proposed technique. The proposed TDDRPS technique is compared with the conventional operation of the CCM inverter for 1) change in active power of the CCM inverter (due to change in solar irradiation), 2) change in load power demand. Experimentally, it is shown that the proposed TDDRPS technique reduces ΔT_j when $\Delta T_j \neq 0$ and for $\Delta T_j = 0$ it distributes T_{jm} uniformly between the inverters thereby improving the collective lifetime of the PE converters in a microgrid.

References

[1] J. Falck, C. Felgemacher, A. Rojko, M. Liserre, and P. Zacharias, "Reliability of power electronic systems: An industry perspective," *IEEE Ind. Electron. Mag.*, vol. 12, no. 2, pp. 24–35, Jun. 2018.

[2] S. Yang, A. Bryant, P. Mawby, D. Xiang, L. Ran, and P. Tavner, "An industry-based survey of reliability in power electronic converters," *IEEE Trans. Ind. Appl.*, vol. 47, no. 3, pp. 1441–1451, May/Jun. 2011.

[3] D. Zhou, H. Wang, and F. Blaabjerg, "Mission profile based system-level reliability analysis of DC/DC converters for a backup power application," *IEEE Trans. Power Electron.*, vol. 33, no. 9, pp. 8030–8039, Sep. 2018.

[4] P. D. Reigosa, H. Wang, Y. Yang, and F. Blaabjerg, "Prediction of bond wire fatigue of IGBTS in a PV inverter under a long-term operation," *IEEE Trans. Power Electron.*, vol. 31, no. 10, pp. 7171–7182, Oct. 2016.

[5] Y. Song and B. Wang, "Survey on reliability of power electronic systems," *IEEE Trans. Power Electron.*, vol. 28, no. 1, pp. 591–604, Jan. 2013.

[6] I. F. Kovacevic-Badstuebner, J. W. Kolar, and U. Schilling, "Modelling for the lifetime prediction of power semiconductor modules," pp. 3–137, Dec. 2015, doi: 10.1049/PBPO080E_ch5.

[7] V. Raveendran, M. Andresen, and M. Liserre, "Improving onboard converter reliability for more electric aircraft with lifetime-based control," *IEEE Trans. Ind. Electron.*, vol. 66, no. 7, pp. 5787–5796, Jul. 2019.

[8] M. Andresen, V. Raveendran, G. Buticchi, and M. Liserre, "Lifetime-based power routing in parallel converters for smart transformer application," *IEEE Trans. Ind. Electron.*, vol. 65, no. 2, pp. 1675–1684, Feb. 2018.

[9] S. Peyghami, P. Davari, and F. Blaabjerg, "System-level reliability-oriented power sharing strategy for DC power systems," *IEEE Trans. Ind. Appl.*, vol. 55, no. 5, pp. 4865–4875, Sep./Oct. 2019.

[10] J. Jiang, S. Peyghami, C. Coates, and F. Blaabjerg, "A decentralized reliability-enhanced power sharing strategy for PV-based microgrids," *IEEE Trans. Power Electron.*, vol. 36, no. 6, pp. 7281–7293, Jun. 2021.

[11] K. Ma, M. Liserre, and F. Blaabjerg, "Reactive power influence on the thermal cycling of multi-MW wind power inverter," *IEEE Trans. Ind. Appl.*, vol. 49, no. 2, pp. 922–930, Mar./Apr. 2013.

[12] Y. Wang, D. Liu, P. Liu, F. Deng, D. Zhou, and Z. Chen, "Lifetime-oriented droop control strategy for AC islanded microgrids," *IEEE Trans. Ind. Appl.*, vol. 55, no. 3, pp. 3252–3263, May/Jun. 2019.

[13] J. He, Y. Li, B. Liang, and C. Wang, "Inverse power factor droop control for decentralized power sharing in series-connected-microconverters-based islanding microgrids," *IEEE Trans. Ind. Electron.*, vol. 64, no. 9, pp. 7444–7454, Sep. 2017.
[14] F. Gao, S. Bozhko, A. Costabeber, G. Asher, and P. Wheeler, "Control design and voltage stability analysis of a droop-controlled electrical power system for more electric aircraft," *IEEE Trans. Ind. Electron.*, vol. 64, no. 12, pp. 9271–9281, Dec. 2017.
[15] T. Dragičević, X. Lu, J. C. Vasquez, and J. M. Guerrero, "DC microgrids-part I: A review of control strategies and stabilization techniques," *IEEE Trans. Power Electron.*, vol. 31, no. 7, pp. 4876–4891, Jul. 2016.
[16] Y. Wang, P. Liu, D. Liu, F. Deng, and Z. Chen, "Enhanced hierarchical control framework of microgrids with efficiency improvement and thermal management," *IEEE Trans. Energy Convers.*, vol. 36, no. 1, pp. 11–22, Mar. 2021.
[17] M. Musallam and C. M. Johnson, "An efficient implementation of the rainflow counting algorithm for life consumption estimation," *IEEE Trans. Reliab.*, vol. 61, no. 4, pp. 978–986, Dec. 2012.
[18] M. F. Ashby and D. R. H. Jones, "Chapter 18 - fatigue design," in *Engineering Materials 1—An Application to Properties, Applications, and Design*, 4th ed., M. F. Ashby and D. R. Jones, Eds. Amsterdam, The Netherlands: Elsevier, 2012, pp. 265–285. [Online]. Available: http://materialstandard.com/wp-content/uploads/2019/06/AshbyEngineering-Materials-1.pdf
[19] J. Colmenares, D.-P. Sadik, P. Hilber, and H.-P. Nee, "Reliability analysis of a high-efficiency SiC three-phase inverter," *IEEE Trans. Emerg. Sel. Topics Power Electron.*, vol. 4, no. 3, pp. 996–1006, Sep. 2016.
[20] A. Anurag, Y. Yang, and F. Blaabjerg, "Thermal performance and reliability analysis of single-phase PV inverters with reactive power injection outside feed-in operating hours," *IEEE Trans. Emerg. Sel. Topics Power Electron.*, vol. 3, no. 4, pp. 870–880, Dec. 2015.

Anubrata Das (Student Member, IEEE) received the B.E. degree in electrical engineering from Bengal Engineering and Science University, Shibpur, (IIEST Shibpur), India, in 2013. He is currently working toward the Ph.D. degree in electrical engineering with the Indian Institute of Technology (IIT) Kanpur, Kanpur, India.

He was associated with ABB India Ltd., Bangalore, India, from 2013 to 2015. His research interests include modeling and control of microgrid, renewable energy integration.

Yugal Gupta (Student Member, IEEE) received the B.Tech. degree in electrical engineering from the Indian Institute of Technology Roorkee, Roorkee, India, in 2018. He is currently working toward the Ph.D. degree in electrical engineering with Virginia Tech University, Blacksburg, VA, USA.

Previously, he was a Research Fellow with the Indian Institute of Technology Kanpur, Kanpur, India. His research interests include power conversion and control techniques.

Sandeep Anand (Senior Member, IEEE) received the B.Tech. and Ph.D. degrees in electrical engineering from the Indian Institute of Technology Bombay, Mumbai, India, in 2007 and 2013, respectively.

He was previously with Emerson Network Power, Mumbai, India, and Cosmic Circuits Pvt., Ltd., Bengaluru, India. He was an Associate Professor with the Indian Institute of Technology, Kanpur, India, from 2013 to 2020. He is currently an Associate Professor with the Indian Institute of Technology Bombay. His research interests include reliability of power electronic circuits, gallium nitride (GaN)-based converters and control of converters interfacing alternate sources of energy.

Soumya Ranjan Sahoo (Senior Member, IEEE) received the B.Tech. degree in electrical engineering from VSSUT, Burla, India, in 2008, and the M.Tech. and Ph.D. degrees in systems and control engineering from the Indian Institute of Technology Bombay, Mumbai, India, in 2013.

He is currently with the Faculty of Electrical Engineering, Indian Institute of Technology Kanpur, Kanpur, India. His research interests include control of unmanned vehicles, multiagent systems, coordinated control, and its applications to aerospace and electrical systems.